ACS Catalysis

Research Article

Cite This: ACS Catal. 2019, 9, 8682−8692

pubs.acs.org/acscatalysis

Effect of Ionic Liquid Modification on the ORR Performance and Degradation Mechanism of Trimetallic PtNiMo/C Catalysts

Michael George,[†] Gui-Rong Zhang,*[,†] Nicolai Schmitt,[†] Kai Brunnengräber,[†] Daniel J. S. Sandbeck,[‡,§] Karl J. J. Mayrhofer,[‡,§] Serhiy Cherevko,[‡] and Bastian J. M. Etzold*[,†]

[†]Ernst-Berl-Institut für Technische und Makromolekulare Chemie, Technische Universität Darmstadt, 64287 Darmstadt, Germany

[‡]Helmholtz-Institute Erlangen-Nürnberg for Renewable Energy (IEK-11), Forschungszentrum Jülich GmbH, 91058 Erlangen, Germany

[§]Department of Chemical and Biological Engineering, Friedrich-Alexander-Universität Erlangen-Nürnberg, 91058 Erlangen, Germany

Supporting Information

ABSTRACT: Ionic liquids (ILs) modification, following the concept of "solid catalyst with ionic liquid layer (SCILL)", has been demonstrated to be an effective approach to improving both activity and stability of Pt-based catalysts for the oxygen reduction reaction. In this work, the SCILL concept has been applied to a trimetallic PtNiMo/C system, which has been documented recently to be significantly advantageous over the benchmark PtNi-based catalysts for oxygen reduction. To achieve this, two hydrophobic ILs ([BMIM][NTF2] and [MTBD][BETI]) were used to modify PtNiMo/C with four IL-loading amounts between 7 and 38 wt %. We found that the Pt mass activity (@0.9 V) could be improved by up to 50% with [BMIM][NTF2] and even 70% when [MTBD][BETI] is used. Exceeding a specific IL loading amount, however, leads to a mass transport related activity drop. Moreover, it is also disclosed that both ILs can effectively suppress the formation of nonreactive oxygenated species, while at the same time imposing little effect on the electrochemical active surface area. For a deeper understanding of the degradation mechanism of pristine and IL modified PtNiMo/C, we applied identical location transmission electron microscopy and *in situ* scanning flow cell coupled to inductively coupled plasma mass spectrometry techniques. It is disclosed that the presence of ILs has selectively accelerated the dissolution of Mo and eventually results in a more severe degradation of PtNiMo/C. This shows that future research needs to identify ILs that prevent the Mo dissolution to leverage the potential of the IL modification of PtNiMo catalysts.

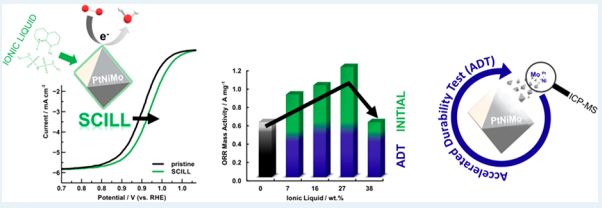

KEYWORDS: *oxygen reduction, electrocatalysis, PtNiMo catalyst, ionic liquid, metal dissolution, stability*

1. INTRODUCTION

Low-temperature fuel cells (LTFCs) are gaining increasing attention in both the public and science community as they offer a promising option in the future clean energy scenario with particularly important applications in the automotive sector.[1−3] Carbon supported Pt-based nanoparticles still represent the state-of-the-art catalyst for both the anodic hydrogen oxidation and cathodic oxygen reduction reaction (ORR) in LTFCs. However, high Pt loadings are required to accelerate the sluggish ORR at the cathode, and these along with the resultant high cost of electrode catalysts (accounting for up to 55% of the total cost of a LTFC) greatly impede the market-penetration of LTFC technology.[4−7] Intensive efforts have been devoted to minimize the usage of expensive Pt by developing innovative catalysts with superior activity.[8] Alloying Pt with other base metals (e.g., Fe, Co, Ni) has been undoubtedly the most efficient strategy so far for this purpose. Specifically, PtNi alloyed nanoparticles terminated with (111) facets are probably the most studied systems since the benchmark work of Stamenkovic et al., who reported 2 orders of magnitude higher ORR activity (vs Pt/C) obtained on an alloyed $Pt_3Ni(111)$ model catalyst.[9−11] Despite the great promise and numerous successes in attaining remarkably high ORR activity over PtNi-based catalysts, their durability performance is still far from satisfying because of the preferred leaching of Ni and associated surface restructuring under voltage cycling conditions,[12,13] which is induced by frequent start/stop events and load variations of LTFC devices.[14−16] In view of this, many attempts have been made to suppress the degradation of PtNi catalysts without compromising their high initial activity. Among other options, incorporation of a third metal could achieve the desired stabilizing effect combined with a high ORR activity and can be seen as a game changer in the field. Henceforth, doping PtNi with various transition metals such as Cu,[17] Fe,[18] Rh,[12] Co,[19−21] or Mo[22−24] has become the favored strategy for preventing Ni dissolution.

Received: April 30, 2019
Revised: July 15, 2019
Published: August 12, 2019

DOI: 10.1021/acscatal.9b01772
ACS Catal. 2019, 9, 8682−8692

Especially Mo-doped PtNi could stand out from various PtNiM-alloys, by exhibiting not only an improved voltage-cycling stability but also an exceptionally high ORR activity (7 A mg_{Pt}^{-1}, @0.90 V).[23] The presence of Mo in PtNi catalysts could take effect to keep the shape and surface composition of PtNi nanoparticles by stabilizing under-coordinated Pt sites and increasing the concentration of subsurface Ni atoms.[22,24]

Surface modification with a subtle amount of hydrophobic ionic liquid (IL) has recently emerged as another efficient approach to enhancing the performance of Pt catalysts toward ORR.[25−28] This method was initiated in 2007 in the heterogeneous catalysis community, by reporting that the reaction selectivity of Ni catalyzed sequential hydrogenation of diene was dramatically altered after coating the catalyst with IL.[29] Thereafter the term of "solid catalyst with ionic liquid layer (SCILL)" was coined for such a concept.[29] In 2010, Erlebacher et al. reported that the similar SCILL concept could be applied to an electrocatalyst, and they found that the ORR activity of porous PtNi was improved by 2 to 3 times after IL modification.[25] We have also demonstrated that modifying a conventional Pt/C catalyst using a hydrophobic IL [MTBD]-[NTF2] can efficiently boost the activity for ORR, and the boosting effect is highly sensitive to the IL filling degrees in the pores of the catalysts.[27] The stabilizing effect of IL ([MTBD]-[NTF2]) was also disclosed within this work, which was attributed to the electrostatic protection effect and suppressed carbon corrosion.[27] More recently, we disclosed that conventional and inexpensive imidazolium based ILs were also capable to improve Pt/C catalyst in terms of both activity and stability.[30,31] By systematically varying the side chain lengths of the imidazolium cations ($[C_nC_1\,im][NTf_2]$, n = 2, 4, 6, 10), a distinct dependence of catalytic activity of Pt toward ORR on the side chain length was identified. The highest activity is obtained using an IL with medium chain length (n = 4), as a counterbalance between higher hydrophobicity to more efficiently suppress the formation of oxygenated species and more severely hindered accessibility of Pt sites with elongation of side chain length of ILs.[31] It is also unambiguously confirmed that the IL phase can stabilize Pt catalysts by lowering the Pt dissolution rate, based on the combined identical location transmission electron microscopy (TEM) and *in situ* scanning flow cell coupled to an inductively coupled plasma mass spectrometry (SFC-ICP-MS) analyses.[31] These successful attempts verify the feasibility of improving both the electrochemical activity and stability of Pt/C catalysts by fabricating SCILL samples. However, it remains a mystery about whether this methodology can be transferred from monometallic Pt to more practical relevant multimetallic Pt-based alloy catalysts with sophisticated structures.

To this end, here in the current work, the SCILL concept will be applied to a cutting edge ORR catalyst, i.e., trimetallic PtNiMo/C, which represents so far one of the most efficient ORR catalysts in terms of both activity and stability.[24,32] The two most promising ILs, [BMIM][NTF2] and [MTBD]-[BETI], were used for the modifications, with IL loading amounts on the resultant SCILL samples systematically varied from 7 to 38 wt %. We aim to fill the knowledge gap about whether the activity of the cutting edge PtNiMo/C catalyst can still be boosted and more importantly whether the appealing stabilizing effect of IL modification on the monometallic Pt catalyst can be maintained in the presence of base metals. Furthermore, the degradation mechanism of the pristine and IL modified trimetallic catalysts is comprehensively investigated based on identical location TEM and *in situ* SFC-ICP-MS analyses. On one hand, we found that the presence of IL could boost the ORR performance on these practically relevant PtNiMo/C electrocatalysts, and the boosting effect is sensitive to the exact loading amount of ILs, while on the other hand, we discovered that the ILs could accelerate the leaching of Mo in the catalysts, which compromises the stabilization effect of Mo on the catalysts and therefore leads to a worse durability performance compared to pristine counterparts. These findings would shed new light on the role of ILs in modifying the structural as well as catalytic properties of a solid catalyst and would also have great implications for developing other high-performing catalytic systems following the SCILL concept.

2. EXPERIMENTAL SECTION

2.1. Materials. $Pt(acac)_2$ (98%), $Ni(acac)_2$ (95%), $Mo(CO)_6$ (99%), $HClO_4$ (70 wt %), [BMIM][NTF2] (98%), and 7-methyl-1,5,7-triazabicyclo[4.4.0]dec-5-ene ([MTBD], 98%) were purchased from Sigma-Aldrich. *N*,*N*-Dimethylformamide (99.8+%) and benzoic acid (99%) were purchased from Alfa Aesar. Lithium bis(perfluoroethylsulfonyl)imide (99%) was purchased from IoLiTec GmbH. All chemicals were used as received without further purification. Deionized water (<1.1 $\mu S\ cm^{-1}$) was supplied by VWR chemicals and was used for the prepartion of all aqueous solutions.

2.2. Synthesis of [MTBD][BETI] IL. [MTBD][BETI] was synthesized from 7-methyl-1,5,7-triazabicyclo[4.4.0] dec-5-ene [MTBD] and the lithium salt lithium bis-(pentafluoroethylsulfonyl)imide Li[BETI] according to the procedure described by Luo et al. The detailed synthetic procedure can be found in the Supporting Information. The purity of the resulting IL was characterized by ^1H NMR analysis (Figure S1).

2.3. Synthesis of PtNiMo/C Catalyst. The synthesis of carbon supported PtNiMo catalyst was carried out by employing a surfactant free solvothermal method following literature procedures.[32−34] Detailed information can be found in the Supporting Information.

2.4. Synthesis of PtNiMo/C SCILL System. The modification of the catalyst with ILs was conducted as described in our previous works: 40 mg of catalyst was mixed with 10 mL of isopropanol (ultrapure) containing a specific amount of IL in order to achieve 7, 16, 27, or 38 wt % loading on the as-prepared SCILL samples, and the loading amount of IL is defined as

$$\text{wt\%IL} = \frac{m_{\text{IL}}}{m_{\text{catalyst}} + m_{\text{IL}}}$$

where m_{IL} and m_{catalyst} refer to the masses of IL and PtNiMo/C, respectively. A typically synthesis procedure for a SCILL system is as follows: The mixture was stirred for at least 30 min and ultrasonicated for another 30 min before the solvent was slowly removed by rotary evaporation (40 °C, 120 mbar), followed by further evaporation at 10 mbar. Finally, the sample was dried under vacuum at 80 °C. In this work we tested an imidazolium- ([BMIM][NTF2]) and a triazabicyclodecene-based ([MTBD][BETI]) IL. The structural formulas can be seen in Figure 1.

2.5. Instrumentation. The exact loadings of Pt, Ni, and Mo on the samples were determined using inductively coupled plasma optical emission spectrometry (ICP-OES, Optima 2000DV, *PerkinElmer*). The powder X-ray diffraction (XRD)

DOI: 10.1021/acscatal.9b01772
ACS Catal. 2019, 9, 8682−8692

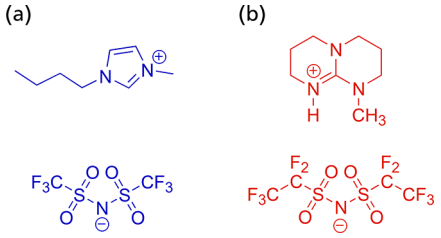

Figure 1. Structural formulas of (a) [BMIM][NTF2] and (b) [MTBD][BETI].

patterns were collected on a StadiP (*Stoe*) using a Ge(111) monochromator with Cu Kα radiation (λ = 1.54060 Å). ^{1}H NMR spectra of the ILs were recorded on an Advance III spectrometer (Bruker), using DMSO-d_6 as solvent. High resolution TEM and STEM images were recorded using a JEM2100F (JEOL) with a field emission gun operating at a nominal acceleration voltage of 200 kV. Energy dispersive X-ray (EDX) spectroscopy line-scan measurements were performed in STEM mode with an X-ray detector (X-max80, Oxford Instruments). Identical-location TEM was carried out using a holey-carbon finder-grid (QUANTIFOIL G200F1). More details about the sample preparation and TEM measurements can be found in the Supporting Information.

2.6. Electrochemical Measurements. Electrochemical measurements were carried out on a PARSTAT Multichannel Potentiostat (PMC-1000, AMETEK) which is controlled by VersaStudio software. A leak-free double-junction Ag/AgCl electrode (Aldrich) was used as reference electrode and a Pt wire (PINE) as counter electrode. All potentials reported in this work were calibrated against a reversible hydrogen electrode (RHE) using hydrogen evolution-oxidation reaction on a Pt electrode. A glassy carbon rotating disk electrode (GC-RDE, 5 mm diameter, PINE) was used as the working electrode. Further details on the electrochemical measurements are summarized in the Supporting Information.

Electrochemical dissolution tests for Pt, Ni, and Mo were carried out on an *in situ* scanning flow cell coupled to an inductively coupled plasma mass spectrometer (SFC-ICP-MS) (NexION 300X, PerkinElmer) as described in previous works.[35,36] The ink preparation and dropcasting process followed a similar procedure to the RDE experiments, with slight modifications necessary for the SFC-ICP-MS measurements. A glassy carbon plate (SIGRADUR G, HTW) was polished with 0.05 μm alumina paste (Stuers), with repeated polishing until ultrapure water easily beaded off while rinsing. A catalyst ink was prepared with ultrapure water, 25% isopropanol, and 5% Nafion solution. The ionomer/carbon ratio was held at 0.35 g g^{-1}, while an appropriate volume was used to obtain a final loading of 10 μg_{Pt} cm^{-2} based on a final working electrode area of 0.01 cm^2 from dropcast spots of 0.3 μL on the glassy carbon plate. The suspension was sonicated with a horn sonifier and ice cooling, and then an aliquot was immediately diluted with ultrapure water immediately prior to dropcasting to obtain a 12.5% isopropanol, as lower alcohol contents are required for dropcasting on GC plates without a PTFE shroud.

3. RESULTS AND DISCUSSION

3.1. Catalyst Characterization. The trimetallic PtNiMo colloidal nanoparticles were synthesized via a surfactant-free solvothermal approach. The resulting nanoparticles were immobilized on high surface area carbon black (Ketjenblack EC-300J) to obtain PtNiMo/C. ICP-OES analysis was conducted to determine sample compositions and offered a Pt-loading of 17.3 wt % and a final atomic composition of Pt:Ni:Mo = 1:0.44:0.01. From TEM analysis (Figure 2a–b) it can be seen that nanoparticles adopt a unique octahedral shape and uniformly distribute over the carbon support without any severe aggregation. The statistical analysis of over 300 randomly selected nanoparticles reveals that the average particle size of PtNiMo is 6.0 ± 0.9 nm. As displayed in Figure 2c, the XRD analysis reveals that all the diffraction peaks shifted toward higher angles relative to those of the reference Pt, which indicates a contracted Pt lattice due to the alloying of Pt with base metals (i.e., Ni). No additional peak from either Ni or Mo species can be detected in the XRD pattern, confirming the formation of a single Pt-based alloy phase.

3.2. Electrochemical Characterization. The thin-film RDE technique was used to analyze the electrochemical properties of the catalysts. Figure 3 shows the resulting CV curves of the pristine and IL modified samples. All catalysts exhibit the characteristic signals of H adsorption/desorption over Pt surfaces in the potential range of 0.05–0.4 V and surface oxidation of Pt (i.e., formation of Pt–OH$_{ad}$) in the

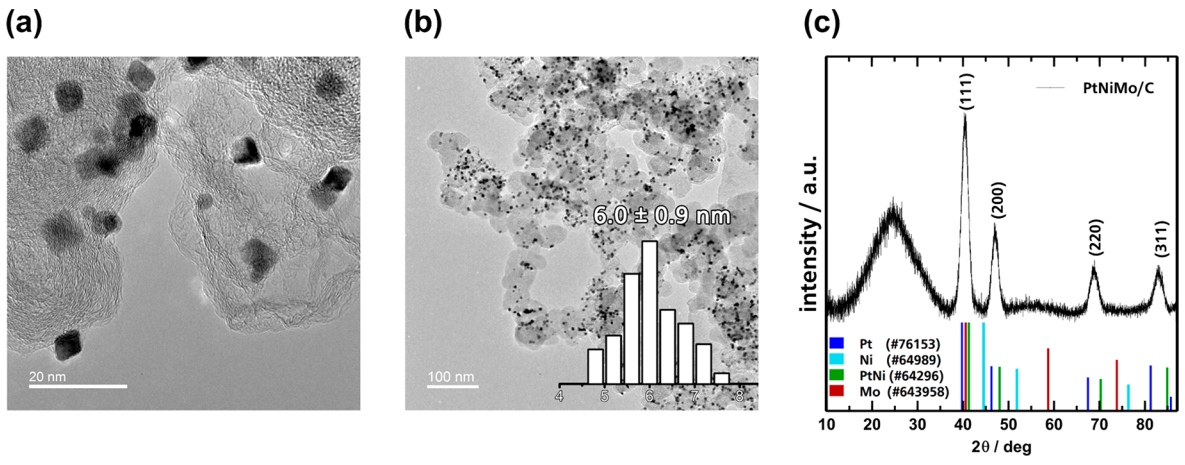

Figure 2. (a–b) TEM images of PtNiMo nanoparticles supported on Ketjenblack EC300J. Over 300 nanoparticles were selected randomly for the statistical analysis. (c) XRD patterns of PtNiMo/C with assigned diffraction peaks from Inorganic Crystal Structure Database (ICSD).

DOI: 10.1021/acscatal.9b01772
ACS Catal. 2019, 9, 8682–8692

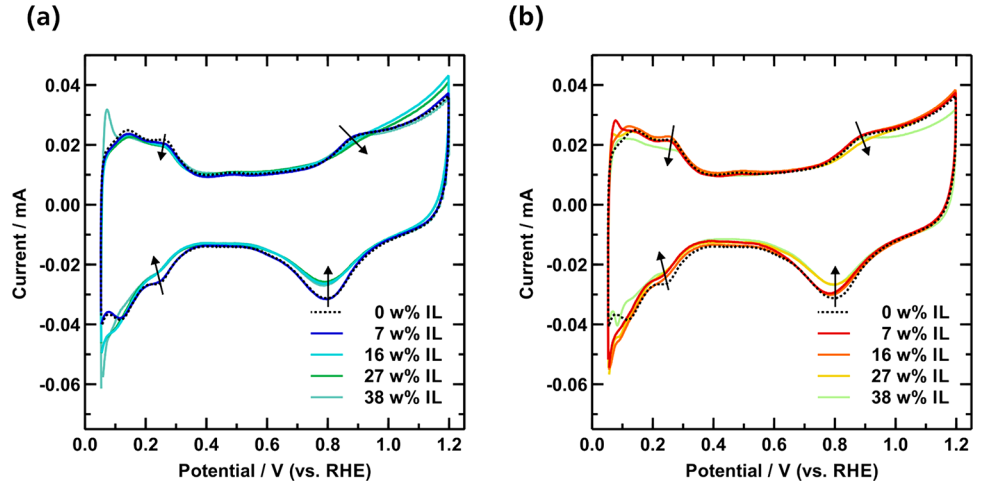

Figure 3. Cyclic voltammetry curves of pristine and IL modified PtNiMo/C with varied IL loading amounts of (a) [BMIM][NTF2] and (b) [MTBD][BETI], recorded in N_2-saturated 0.1 M $HClO_4$ electrolyte (scan rate: 20 mV s^{-1}).

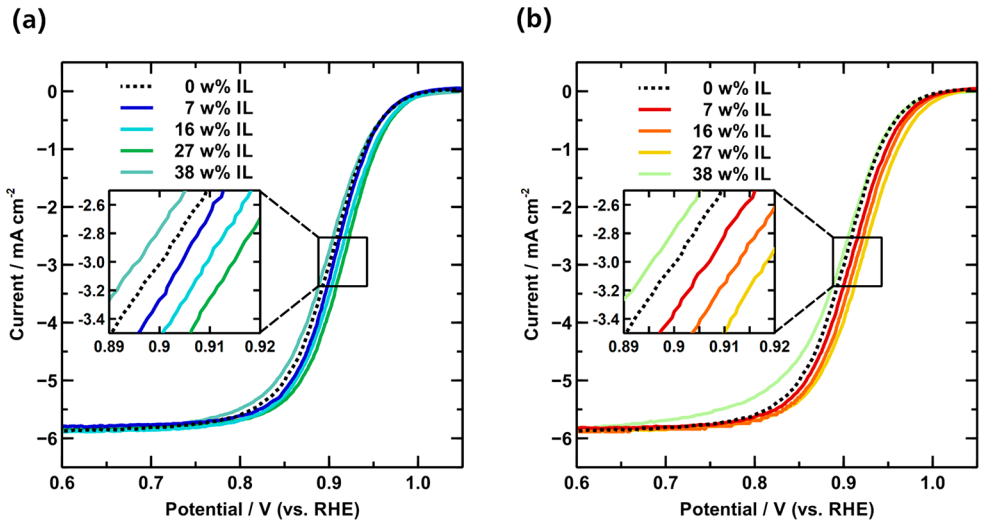

Figure 4. ORR polarization curves of pristine and IL-modified PtNiMo/C with varied IL loading amounts of (a) [BMIM][NTF2] and (b) [MTBD][BETI], recorded in O_2 saturated 0.1 M $HClO_4$ solution (20 mV s^{-1}).

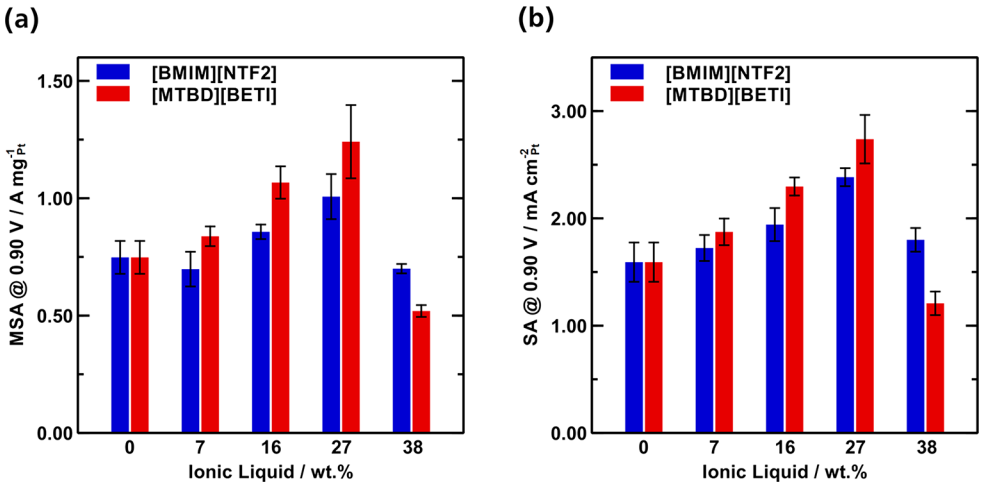

Figure 5. Comparison of (a) mass specific activity and (b) specific activity of pristine and IL-modified PtNiMo/C catalysts at 0.9 V.

potential range of 0.8−1.0 V. Only minor changes can be observed in the CVs after the introduction of IL to the PtNiMo/C catalysts. In the H-adsorption/desorption regime a slight suppression of the corresponding peaks can be noted (illustrated by arrows). However, the hereby calculated electrochemically active surface area ($ECSA_H$) does not suffer

DOI: 10.1021/acscatal.9b01772
ACS Catal. 2019, 9, 8682−8692

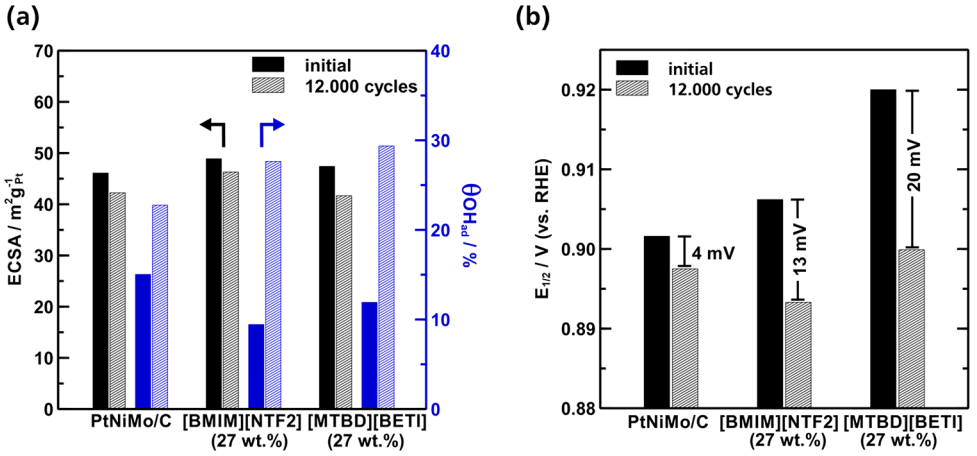

Figure 6. Changes in (a) ECSA, adsorption of oxygenated species and (b) half-wave potential of PtNiMo/C with/without ILs after 12,000 potential cycles with a scan rate of 50 mV s^{-1} between 0.6 and 1.1 V. The IL loading is 27 wt % for both SCILL samples.

from a drastic loss and decreases only slightly from 45 to 39 m^2 g^{-1}_{Pt}. This trend can also be confirmed by the results obtained from CO-stripping experiments ($ECSA_{CO}$), which are in good agreement to the $ECSA_H$ (see Figure S2). These results obtained from cyclic voltammetry prove that most of the active sites of PtNiMo/C are not being blocked by the ILs and are still accessible to protons. Apart from the H-regime a closer look at the OH_{ad}-regime (0.8−1.0 V) shows that the Pt−OH oxidation as well as the corresponding reduction peak are incrementally suppressed, when the amount of IL is increased. This protection of active sites from forming nonreactive oxygenated species can be observed for both ILs and is in line with our previous results.[26,27]

The electrocatalytic properties of the pristine and IL modified PtNiMo/C catalysts toward the ORR were analyzed by using the thin film RDE technique. The resulting anodic polarization curves are shown in Figure 4. By examining the mixed kinetic-diffusion controlled region (0.85−0.95 V), a positive shift of the half wave potential ($E_{1/2}$) can always be found on the IL modified catalysts with IL-loading amounts up to 27 wt %, verifying that the presence of ILs can also boost the ORR kinetics over these PtNiMo/C catalysts. This boosting effect can be observed for both ILs, while it is more pronounced for [MTBD][BETI] (+14 mV) than for [BMIM]-[NTF2] (+8 mV). However, further increasing the IL loading to 38 wt %, leads to a reversal of this trend and a negative shift in $E_{1/2}$.

A more detailed view on the development of the ORR activity is received after quantifying the specific activities (SA) and mass-specific activities (MSA) at 0.9 V, as shown in Figure 5. Hereby, it becomes clear that the ORR activity is improved for both ILs when the IL-loading is increased up to 27 wt %. Specifically, the MSA values of Pt are increased by 50% and 70% when [BMIM][NTF2] and [MTBD][BETI] are in use, respectively. The highest ORR activity with a MSA over 1.2 A mg^{-1}_{Pt} and a SA of almost 3 mA cm^{-2}_{Pt} was reached by using 27% of [MTBD][BETI]. Interestingly, higher IL-loadings (38 wt %) have a negative impact on the ORR-performance regardless of the ILs being used, and in the case of [MTBD][BETI], the performance is even inferior to that of the pristine counterpart. This result is not surprising since similar IL-loading dependent behavior of ORR performance has already been observed on Pt/C catalysts and also noble metal free Fe−N−C catalysts, which can be rationalized by the counterbalance between more efficient IL boosting effect and higher resistance of O_2 diffusion within the IL phase.[27,37]

3.3. Durability Tests. Furthermore, we applied accelerated degradation test (ADTs) to probe the possible influence of IL modification on the durability of the catalysts. We chose an ADT protocol, which is widely used for evaluating the durability of Pt-based catalysts using repeated voltammetric cycling in the potential range of 0.6 to 1.1 V. Since this anodic vertex potential is not sufficient to trigger severe carbon corrosion, the possible catalyst degradation would mainly stem from structural changes of the nanoparticles during the test.[16,38,39] Figure 6 compares ECSA, coverage of nonreactive oxygenated species ($\theta_{OH,ad}$), and $E_{1/2}$ for the pristine and 27 wt % SCILL samples before and after the ADT. The pristine PtNiMo/C catalyst offers convincing durability results, as 90% of its initial ECSA and MSA was retained after 12,000 cycles. The $E_{1/2}$ is shifted by only −4 mV over the cycling period, leading to a MSA of 0.5 A mg^{-1}_{Pt}, which proves the successful stabilization effect of the Mo-doping.

Surprisingly, the IL modified PtNiMo/C-SCILL samples show a significantly higher loss in the ORR activity than the pristine sample. The $E_{1/2}$ is shifted negatively by 13 mV for PtNiMo-[BMIM][NTF2] and even 20 mV for PtNiMo-[MTBD][BETI] (Figures 6b and S4). Interestingly, it turns out that the degraded SCILL samples exhibit similar end activity (0.5−0.6 A mg^{-1}_{Pt}) to the pristine PtNiMo/C. It appears that the similar end activities of the ADT result from either oxidative decomposition or loss of the IL during potential cycling. However, ILs are known to be extraordinarily stable in terms of their electrochemical window.[40] For example [BMIM][NTF2] was tested to be stable between −2.0 and 2.7 V (vs Ag).[41] Although it is also known that the presence of catalytically active Pt and even water can reduce the upper potential limit of ILs,[41,42] it should be emphasized that the carbon support is the more vulnerable part in terms of the oxidation stability of a SCILL catalyst. As to the possible loss of IL during the ADT, in our previous investigation on Pt/C-[BMIM][NTF2] a high retention of the ORR activity was still observed after the ADT, proving that the [BMIM][NTF2] still remains after applying a rather positive potential of up to 1.4 V (vs RHE).[27] To better clarify this issue, herein we applied STEM-EDX analysis of six different spots (~2 μm spot size) on PtNiMo-[MTBD][NTF2] (27 wt %) before and after the ADT to indisputably prove the presence of IL on the catalyst

DOI: 10.1021/acscatal.9b01772
ACS Catal. 2019, 9, 8682−8692

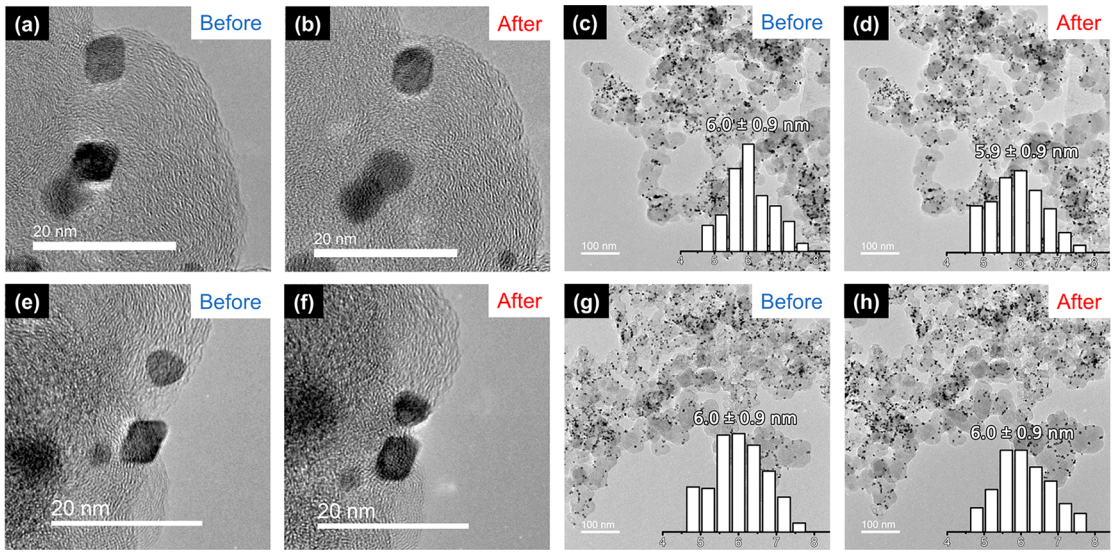

Figure 7. Identical-location TEM images of (a–d) pristine PtNiMo/C and (e–-h) PtNiMo/C with 27 wt % [MTBD][BETI] before and after the ADT (12,000 cycles, 0.6–1.1 V vs RHE, 50 mV s^{-1}).

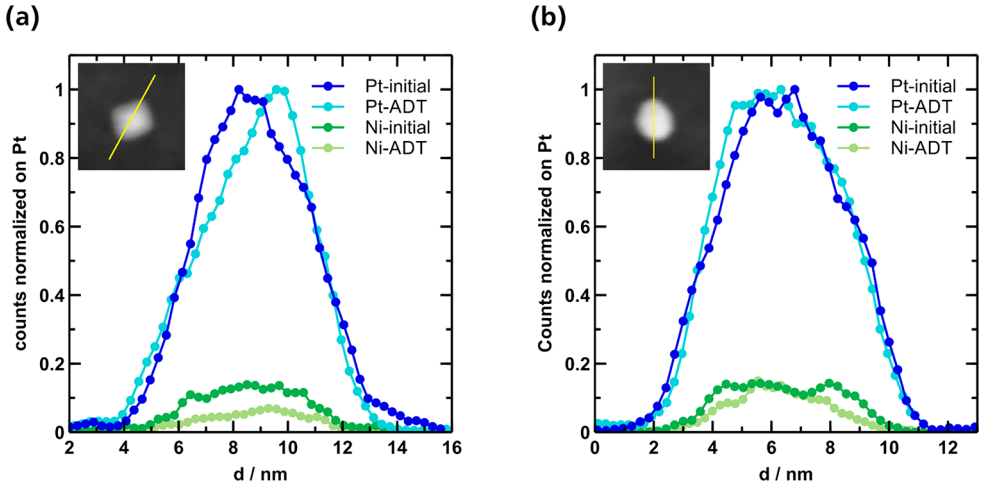

Figure 8. STEM-EDX line scan profiles of individual nanoparticles of (a) PtNiMo/C and (b) PtNiMo/C with 27 wt % [MTBD][BETI] before and after the ADT. The insets show individual nanoparticles before the ADT.

surface even after 12,000 potential cycles. From the EDX spectrum in Figure S6 the expected signals from IL (F and S) can be observed. By comparing the F/Pt ratio, we can present here a piece of strong evidence that no severe loss of IL occurs during the ADT and the amount of IL is still comparable to that of the pristine sample. This result proves that the activity loss of the PtNiMo-SCILL catalysts does not simply stem from loss of IL into the electrolyte. As the ECSA is satisfyingly retained (>92%) for these SCILL samples, the reason for the higher drop in ORR activity seems not to stem from typical degradation mechanisms like coalescence of nanoparticles or Pt dissolution. It can also be noticed that initial $\theta_{OH,ad}$ values on the SCILL samples are lower than that on the pristine PtNiMo/C (Figure 6a), indicating that the presence of IL can to some extent suppress the formation of those nonreactive oxygenated species which is in line with previous works. Nevertheless, the $\theta_{OH,ad}$ values on both SCILL samples have increased by almost 2 times after the ADT, as shown in Figure 6a, while this is not the case for the pristine PtNiMo/C sample. This result implies that the presence of ILs would have induced some significant surface restructuring of PtNiMo/C catalysts during the ADT, which may eventually result in the different degradation behavior of PtNiMo catalysts with/without ILs.

We used identical-location TEM to probe the structural change of pristine and [MTBD][BETI] modified PtNiMo/C before and after the ADT. Herein we disclose that both pristine and SCILL samples undergo comparable changes in particle morphology during the ADT. As displayed in Figure 7, no migration or coalescence of nanoparticles can be observed and the average particle size stays constant at ~6.0 nm. High resolution images in the upper part of Figure 7 reveal, however, that the octahedral shape of the nanoparticles is lost during the ADT and the nanoparticles take an almost spherical shape by truncating the corners of the octahedra. Loss of the octahedral shape is considered as one of the major causes for activity decline of PtNi-nanoparticles, since the surface proportion of the most active (111) facets is reduced. Although Mo-doping is reported to stabilize the octahedral shape by reducing the leaching rate of Ni, we could not observe a full retention of the shape. We also made an attempt to distinguish the composition changes of these two samples before and after ADT by recording STEM-EDX line-scan profiles on individual

DOI: 10.1021/acscatal.9b01772
ACS Catal. 2019, 9, 8682–8692

nanoparticles, as shown in Figure 8. It can be found that the signals from Pt and Ni are distributed evenly over the whole particle, while an obvious reduction in atomic Ni/Pt ratio can be observed for both samples (Figure 8) after ADT. To be specific, the ratio is reduced from 0.14 to 0.10 for the pristine catalyst and from 0.14 to 0.11 for the PtNiMo-[MTBD]-[BETI] sample. A possible change of the Mo concentration in the particles cannot be determined, as the Mo amount is too low to be unambiguously detected. Therefore, other techniques in addition to TEM and STEM-EDX are still needed to clearly distinguish the degradation mechanism of the pristine and SCILL-modified PtNiMo/C.

Close inspection of the CV curves before and after the ADT (Figure S5) indicates that in contrast to the overall decreased H redox signals on the pristine PtNiMo/C after the ADT, both SCILL samples exhibit strengthened H adsorption/desorption peaks at 0.2−0.3 V (highlighted by arrows), which may correspond to the evolvement of (100) facet/steps during the ADT.[43−45] This selective evolvement of specific Pt sites would be a consequence of the promoted Ni-leaching in the presence of ILs. Figure 9 compares the ECSA values of three catalysts at different cycle numbers of the ADT. Starting from the same ECSA level as the pristine catalyst, especially the [BMIM]-[NTF2] modified sample shows a significant ECSA increase (15%) during the first 1000 cycles, followed by an almost linear decline from 56 to 46 m^2 g_{Pt}^{-1}. This result not only explains the high ECSA retention of the SCILL catalyst but also confirms again the dramatic difference in surface restructuring as well as degradation mechanism especially in the beginning of the ADT between the pristine and IL-modified PtNiMo/C catalysts.

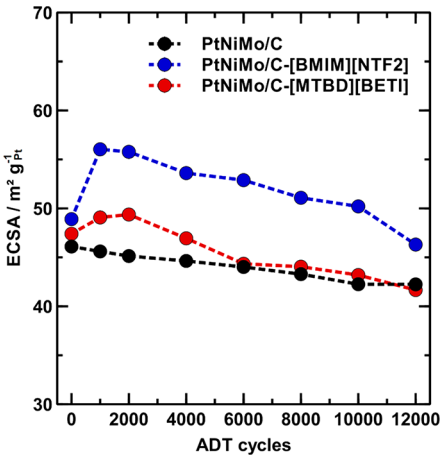

Figure 9. Development of ECSA during the ADT for pristine PtNiMo/C and PtNiMo/C-SCILL catalysts with 27 wt % IL.

In order to better differentiate the degradation behavior of pristine and IL modified PtNiMo/C, we employed the *in situ* SFC-ICP-MS technique to quantify the amounts of dissolved metals during the ADT tests. Figure 10a shows the dissolution profiles of different metals, from which it can be seen that a significant dissolution occurs for all three metals upon the SFC making contact with the catalyst-coated working electrode when the open circuit potential conditions were established. Thereafter, the highest dissolution rate is observed at the beginning of the ADT for all three samples, while the dissolution quickly drops back, as shown in Figure 10a. Figure 10b compares the amounts of dissolved metal in the pristine and SCILL samples, from which it can be seen that the total dissolution amount of Pt is less than 0.25% for all the investigated samples, which agrees with the well maintained ECSA values after ADT (Figure 6a). These results imply that direct Pt dissolution would play a minor role in the degradation process for these samples regardless of the IL modifications. In contrast, the dissolution amounts of Ni and Mo species are over 1 order of magnitude higher than that of Pt, which is not surprising considering their non-noble metal nature. At the same time, it is observed that the dissolution amounts of the base metal components in PtNiMo/C especially of Mo in both SCILL samples are much higher than those of the pristine counterpart. Specifically, the dissolution amounts of Ni and Mo are around 5% and 7%, respectively, on the pristine PtNiMo/C. The dissolution of Ni amounts up to 10% on PtNiMo-[BMIM][NTF2] and 12% on PtNiMo-[MTBD][BETI], and it is remarkable to observe that the dissolution amounts of Mo are as high as 43% and 57% on PtNiMo-[BMIM][NTF2] and PtNiMo-[MTBD][BETI], re-

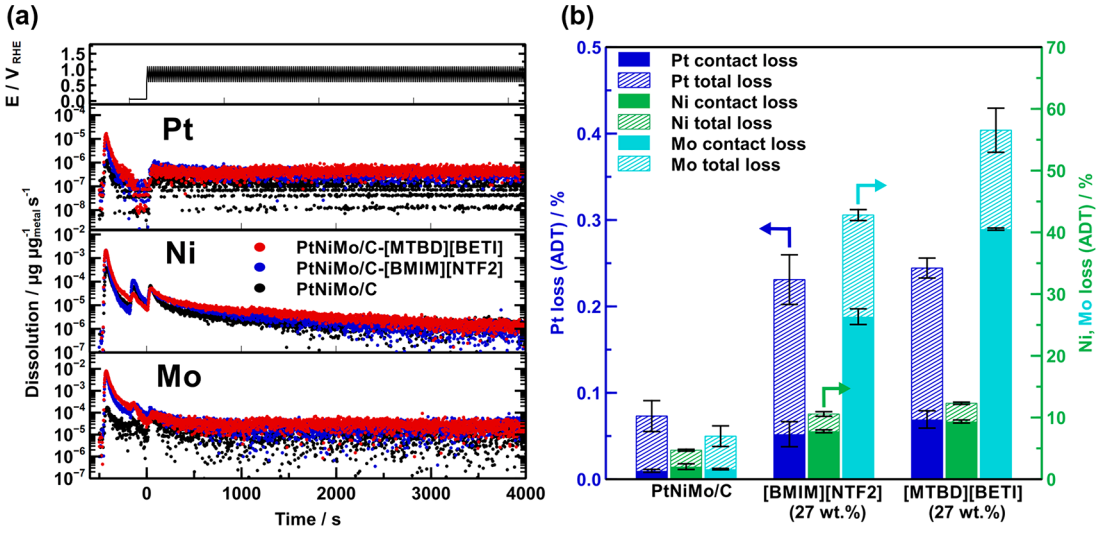

Figure 10. (a) Dissolution profiles and (b) percentage elemental total loss of Pt, Ni, and Mo during ADT of PtNiMo/C and PtNiMo/C-SCILL, determined by SFC-ICP-MS after 200 cycles between 0.6 and 1.1 V (vs RHE) with a scan rate of 50 mV s^{-1}.

DOI: 10.1021/acscatal.9b01772
ACS Catal. 2019, 9, 8682−8692

spectively. These results clearly demonstrate that the presence of IL could aggravate the dissolution of base metal components in PtNiMo/C samples during ADT, which is different from the documented stabilizing effect of IL-modification on the monometallic Pt catalysts.[27,30,31]

To better resolve the metal dissolution under voltage-cycling conditions, we performed additional SFC-ICP-MS experiments with a fresh catalyst coating, by recording metal dissolution profiles during two consecutive CV measurements between 0.05 and 1.5 V with a slow scan rate of 10 mV s^{-1}. As shown in Figure 11, two dissolution peaks can be identified on each

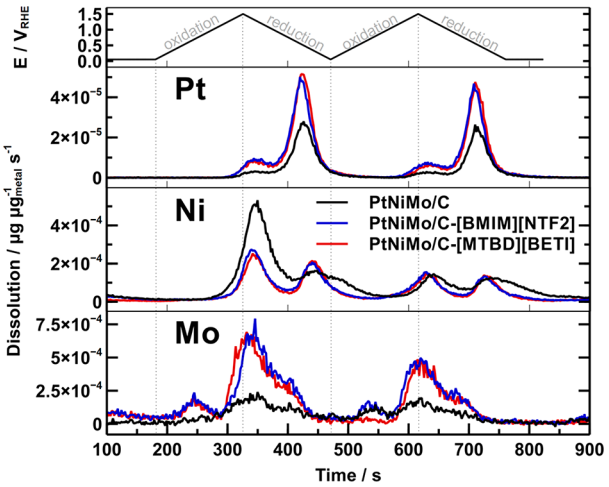

Figure 11. SFC-ICP-MS time and potential resolved dissolution profiles for Pt, Ni, and Mo of pristine PtNiMo/C. Potential window: 0.05−1.5 V (vs RHE); scan rate: 10 mV s^{-1}.

cycle for all three samples. The dissolution of Pt and Ni starts at high potential region (>1.0 V) in the anodic scan, and dominant dissolution peaks emerge in the cathodic scan, which is consistent with previous reports.[36,46] Interestingly, an additional minor dissolution peak for Mo can be observed in the anodic scan at a relatively low potential region, which is absent on the dissolution profiles of both Pt and Ni. This additional peak might arise from dissolution of formed molybdenum oxides species. At the same time, the quantification results in Figure S7 confirm that the dissolution amount of Pt (<0.5%) is less significant than those of Ni and Mo for all three samples. It is also noteworthy that the total dissolution amounts of Ni and Mo on the IL modified PtNiMo/C samples are much higher than that on the pristine sample (Figure S7b). This result verifies again that the introduction of ILs has induced aggravated dissolution of base metal components in a trimetallic PtNiMo/C catalyst.

Based on the above SFC-ICP-MS analyses we can get a clearer picture about the degradation mechanism of PtNiMo/C catalysts with/without IL. Both ILs impose a significant impact on the degradation of PtNiMo/C and are responsible for the more severe activity loss of PtNiMo/C-SCILL catalysts compared to the pristine sample. As mentioned above, the activity drop of the SCILL samples cannot be attributed to the loss of Pt, as only minor amounts of Pt are dissolved during this test (<0.25%), which is in accordance with the high ECSA retention (<92%) after 12,000 potential cycles. The IL induced accelerated dissolution of base metal components, especially the high dissolution of Mo (up to 60%), is likely responsible for the accelerated degradation of the SCILL samples, as Mo is believed to play a crucial role in the stabilization of the alloy by preventing Ni dissolution. Losing this stabilization effect likely leads to dealloying of PtNi and diminishing of the Ni related promotion effect on Pt, as evidenced by the enhanced $\theta_{OH,ad}$ values on both SCILL samples after the ADT.

The last puzzle is to understand the origin of the accelerated dissolution of base metals especially of Mo in the presence of ILs. In aqueous medium, an insoluble passive oxide film tends to form on surfaces of transition metals including Ni[47] and Mo[48−50] under anodic polarization conditions.[51] The passive oxide film can prevent further oxidation or dissolution of these metals even in acidic electrolyte as observed on pristine PtNiMo/C, on which the dissolution amounts of both Ni and Mo are less than 10% after the ADT. Therefore, it appears that the much higher dissolution rates of both Mo and Ni on IL-modified PtNiMo samples stem from the absence of the passive oxide layer. ILs can take effect either by suppressing the formation of the metal oxide layer as observed on Pt-based catalysts,[30,31] or by the high solubilizing power of ILs for metal oxides due to their strong complexing capability toward metal ions.[52−56] To clarify this issue, we performed additional electrochemistry measurements on Mo/C and MoO_3/C samples (10 wt % Mo) with and without [BMIM][NTf2] (30 wt %), as shown in Figures S8 and S9. It can be seen that the oxidation signals at around 0.7 V, stemming from the formation of MoO_3 species,[57] can be clearly identified on all four samples, indicating that the presence of IL has not significantly impeded the formation of oxide layer/species. With increasing the cycle number, the oxidation peak gradually strengthens and then stabilizes on pristine samples, while in contrast, the same oxidation peak rapidly vanishes on the IL modified ones and becomes almost completely invisible after 100 cycles, leaving over a CV curve resembling that of carbon support. These results verify that the presence of IL can accelerate the loss of Mo, and they also infer that the passive metal oxide species can hardly survive in the presence of IL under electrochemical conditions. The same conclusion can also be reached by performing *in situ* SFC-ICP-MS experiments on Mo/C and MoO_3/C with and without IL. As shown in Figure S10, both Mo/C and MoO_3/C exhibit more severe dissolution after the IL modification, and the presence of IL has increased the percentage loss of Mo by 25% and 35%, respectively. These results prove a drastic change in the corrosion resistance of molybdenum species in the presence of IL and provide another piece of evidence that the IL has accelerated the loss of molybdenum species. Similarly, Abbott et al. reported that the passive metal oxide film was less likely to exist in an imidazolium-based IL electrolyte due to the solvation of IL−metal complexes.[51] To clarify whether this is also the reason for higher loss of Ni in the presence of IL, we analyzed the dissolution profiles of Ni over a Mo-free PtNi/C sample using the *in situ* SFC-ICP-MS technique (Figure S11). It is found that (1) the Ni dissolution amount is much higher on PtNi/C (37%) than that on PtNiMo/C (10%), verifying that the presence of Mo can effectively stabilize Ni against dissolution; (2) the presence of IL imposes little effect on the overall dissolution amount of Ni in PtNi/C. Therefore, the higher Ni loss on IL-modified PtNiMo/C samples is more likely a consequence of the accelerated Mo loss in the presence of IL and the associated compromised stabilization effect of Mo. These results lead us to conclude that ILs are capable of selectively solubilizing molybdenum species in trimetallic PtNiMo/C samples due to their strong complexing interaction

DOI: 10.1021/acscatal.9b01772
ACS Catal. 2019, 9, 8682−8692

with ILs, which would not only accelerate the leaching of Mo itself but also compromise its stabilizing effect against Ni dissolution and eventually lead to worse overall stability. In the case of pristine PtNiMo/C, the formation of a passive molybdenum oxide layer, however, will make molybdenum species be better retained under the ADT conditions, and consequently pristine PtNiMo/C sample exhibits a significantly lower total loss of base metals and a superior electrochemical stability to those SCILL samples. Moreover, the presence of IL on metal surfaces may cause localized dealloying and/or adsorbate induced surface segregation of these trimetallic nanoparticles by affecting the surface diffusion coefficients of different metal components,[58−60] which could also contribute to the more dramatic change in the surface structure and eventually the worse durability performance of the SCILL samples. Further extensive microscopic and spectroscopic studies are still required before a more fundamental understanding of accelerated leaching of Mo and Ni in the presence of IL can be achieved.

4. CONCLUSION

In conclusion, the present work proves the boosting effect of ILs toward the ORR on a practically relevant PtNiMo/C. An imidazolium ([BMIM][NTF2]) and a triazabicyclodecene-([MTBD][BETI]) based ILs were used to modify catalysts with IL-loadings ranging between 7 wt % and 38 wt %. Both ILs can bring about activity enhancement by up to 50−70%, which was most pronounced at an IL-loading of 27 wt %. The boosting effect on their ORR activity was shown to be dependent on the choice of IL. Besides, no severe change in the ECSA was observed after the introduction of IL, while the adsorption of oxygenated species could be suppressed. From accelerated durability tests it is observed that the stabilization effect of the Mo-doping was lost after introducing IL to the catalyst. With the help of identical-location TEM we demonstrate that both pristine and IL-modified PtNiMo/C catalysts suffer from loss of their octahedral shape after the ADTs, whereas typical degradation reactions such as migration, agglomeration, or particle detachment were successfully suppressed. *In situ* SFC-ICP-MS analyses indicate that IL would selectively accelerate the dissolution of Mo in PtNiMo/C, which leads to the loss of a stabilization effect of Mo and consequently worse durability of SCILL samples. These findings show that future research needs to identify possibilities to avoid the dissolution of less noble components in Pt-based alloyed ORR catalysts, for instance, by engineering the molecular structure of ILs, with the hope of leveraging the IL-boosting effect without compromising their durability performance.

ASSOCIATED CONTENT

Supporting Information

The Supporting Information is available free of charge on the ACS Publications website at DOI: 10.1021/acscatal.9b01772.

ECSA results from CO-Stripping voltammetry, SA and MSA results at 0.95 V (vs RHE), CVs and polarization curves before and after the ADT, SFC-ICP-MS dissolution profiles, and ^{1}H NMR analysis of the used ILs (PDF)

AUTHOR INFORMATION

Corresponding Authors

*E-mail: g.zhang@tc1.tu-darmstadt.de.
*E-mail: etzold@tc1.tu-darmstadt.de.

ORCID

Gui-Rong Zhang: 0000-0002-1803-153X
Bastian J. M. Etzold: 0000-0001-6530-4978

Notes

The authors declare no competing financial interest.

ACKNOWLEDGMENTS

The authors acknowledge the funding from the European Research Council (ERC) under the European Union's Horizon 2020 research and innovation program (grant agreement No. 681719). We thank Dr. Kathrin Hofmann for performing XRD measurements. We would also like to acknowledge Akzo Nobel Functional Chemicals for providing the Ketjenblack materials.

REFERENCES

(1) Jiao, Y.; Zheng, Y.; Jaroniec, M.; Qiao, S. Z. Design of Electrocatalysts for Oxygen-and Hydrogen-Involving Energy Conversion Reactions. *Chem. Soc. Rev.* **2015**, *44*, 2060−2086.

(2) Guo, S.; Zhang, S.; Sun, S. Optimierte Nanopartikel Katalyse Für Die Sauerstoffreduktionsreaktion. *Angew. Chem.* **2013**, *125*, 8686−8705.

(3) Chan, C. C. The State of the Art of Electric, Hybrid, and Fuel Cell Vehicles. *Proc. IEEE* **2007**, *95*, 704−718.

(4) Tan, X.; Prabhudev, S.; Kohandehghan, A.; Karpuzov, D.; Botton, G. A.; Mitlin, D. Pt-Au-Co Alloy Electrocatalysts Demonstrate Enhanced Activity and Durability Towards Oxygen Reduction Reaction. *ACS Catal.* **2015**, *5*, 1513−1524.

(5) Asset, T.; Job, N.; Busby, Y.; Crisci, A.; Martin, V.; Stergiopoulos, V.; Bonnaud, C.; Serov, A.; Atanassov, P.; Chattot, R.; Dubau, L.; Maillard, F., Porous Hollow PtNi/C Electrocatalysts: Carbon Support Considerations to Meet Performance and Stability Requirements. *ACS Catal.*. **2018**, *8*, 893

(6) Li, K.; Li, X.; Huang, H.; Luo, L.; Li, X.; Yan, X.; Ma, C.; Si, R.; Yang, J.; Zeng, J. One-Nanometer-Thick PtNiRh Trimetallic Nanowires with Enhanced Oxygen Reduction Electrocatalysis in Acid Media: Integrating Multiple Advantages into One Catalyst. *J. Am. Chem. Soc.* **2018**, *140*, 16159−16167.

(7) Zhang, G.-R.; Wöllner, S. Hollowed Structured Ptni Bifunctional Electrocatalyst with Record Low Total Overpotential for Oxygen Reduction and Oxygen Evolution Reactions. *Appl. Catal., B* **2018**, *222*, 26−34.

(8) Wang, Y.-J.; Zhao, N.; Fang, B.; Li, H.; Bi, X. T.; Wang, H. Carbon-Supported Pt-Based Alloy Electrocatalysts for the Oxygen Reduction Reaction in Polymer Electrolyte Membrane Fuel Cells: Particle Size, Shape, and Composition Manipulation and Their Impact to Activity. *Chem. Rev.* **2015**, *115*, 3433−3467.

(9) Stamenkovic, V. R.; Fowler, B.; Mun, B. S.; Wang, G.; Ross, P. N.; Lucas, C. A.; Marković, N. M. Improved Oxygen Reduction Activity on Pt3Ni (111) Via Increased Surface Site Availability. *Science* **2007**, *315*, 493−497.

(10) Choi, S.-I.; Xie, S.; Shao, M.; Odell, J. H.; Lu, N.; Peng, H.-C.; Protsailo, L.; Guerrero, S.; Park, J.; Xia, X.; Wang, J.; Kim, M. J.; Xia, Y. Synthesis and Characterization of 9 nm Pt−Ni Octahedra with a Record High Activity of 3.3 A/mgPt for the Oxygen Reduction Reaction. *Nano Lett.* **2013**, *13*, 3420−3425.

(11) Cui, C.; Gan, L.; Li, H.-H.; Yu, S.-H.; Heggen, M.; Strasser, P. Octahedral Ptni Nanoparticle Catalysts: Exceptional Oxygen Reduction Activity by Tuning the Alloy Particle Surface Composition. *Nano Lett.* **2012**, *12*, 5885−5889.

(12) Beermann, V.; Gocyla, M.; Willinger, E.; Rudi, S.; Heggen, M.; Dunin-Borkowski, R. E.; Willinger, M.-G.; Strasser, P. Rh-Doped Pt−

DOI: 10.1021/acscatal.9b01772
ACS Catal. 2019, 9, 8682−8692

Ni Octahedral Nanoparticles: Understanding the Correlation between Elemental Distribution, Oxygen Reduction Reaction, and Shape Stability. *Nano Lett.* **2016**, *16*, 1719−1725.
(13) Cui, C.; Gan, L.; Heggen, M.; Rudi, S.; Strasser, P. Compositional Segregation in Shaped Pt Alloy Nanoparticles and Their Structural Behaviour During Electrocatalysis. *Nat. Mater.* **2013**, *12*, 765.
(14) Banham, D.; Ye, S. Current Status and Future Development of Catalyst Materials and Catalyst Layers for Proton Exchange Membrane Fuel Cells: An Industrial Perspective. *ACS Energy Letters* **2017**, *2*, 629−638.
(15) Cano, Z. P.; Banham, D.; Ye, S.; Hintennach, A.; Lu, J.; Fowler, M.; Chen, Z. Batteries and Fuel Cells for Emerging Electric Vehicle Markets. *Nat. Energy* **2018**, *3*, 279−289.
(16) Chung, D. Y.; Yoo, J. M.; Sung, Y.-E. Highly Durable and Active Pt-Based Nanoscale Design For fuel-Cell Oxygen-Reduction Electrocatalysts. *Adv. Mater.* **2018**, *30*, 1704123.
(17) Zhang, C.; Sandorf, W.; Peng, Z. Octahedral Pt2CuNi Uniform Alloy Nanoparticle Catalyst with High Activity and Promising Stability for Oxygen Reduction Reaction. *ACS Catal.* **2015**, *5*, 2296−2300.
(18) Li, Y.; Quan, F.; Chen, L.; Zhang, W.; Yu, H.; Chen, C. Synthesis of Fe-Doped Octahedral Pt3Ni Nanocrystals with High Electro-Catalytic Activity and Stability Towards Oxygen Reduction Reaction. *RSC Adv.* **2014**, *4*, 1895−1899.
(19) Arán-Ais, R. M.; Dionigi, F.; Merzdorf, T.; Gocyla, M.; Heggen, M.; Dunin-Borkowski, R. E.; Gliech, M.; Solla-Gullón, J.; Herrero, E.; Feliu, J. M. Elemental Anisotropic Growth and Atomic-Scale Structure of Shape-Controlled Octahedral Pt−Ni−Co Alloy Nanocatalysts. *Nano Lett.* **2015**, *15*, 7473−7480.
(20) Lokanathan, M.; Patil, I. M.; Navaneethan, M.; Parey, V.; Thapa, R.; Kakade, B. Designing of Stable and Highly Efficient Ordered Pt2CoNi Ternary Alloy Electrocatalyst: The Origin of Dioxygen Reduction Activity. *Nano Energy* **2018**, *43*, 219−227.
(21) Zhao, Z.; Feng, M.; Zhou, J.; Liu, Z.; Li, M.; Fan, Z.; Tsen, O.; Miao, J.; Duan, X.; Huang, Y. Composition Tunable Ternary Pt-Ni-Co Octahedra for Optimized Oxygen Reduction Activity. *Chem. Commun.* **2016**, *52*, 11215−11218.
(22) Cao, L.; Mueller, T. Theoretical Insights into the Effects of Oxidation and Mo-Doping on the Structure and Stability of Pt−Ni Nanoparticles. *Nano Lett.* **2016**, *16*, 7748−7754.
(23) Huang, X.; Zhao, Z.; Cao, L.; Chen, Y.; Zhu, E.; Lin, Z.; Li, M.; Yan, A.; Zettl, A.; Wang, Y. M.; Duan, X.; Mueller, T.; Huang, Y. High-Performance Transition Metal−Doped Pt3Ni Octahedra for Oxygen Reduction Reaction. *Science* **2015**, *348*, 1230−1234.
(24) Jia, Q.; Zhao, Z.; Cao, L.; Li, J.; Ghoshal, S.; Davies, V.; Stavitski, E.; Attenkofer, K.; Liu, Z.; Li, M.; Duan, X.; Mukerjee, S.; Mueller, T.; Huang, Y. Roles of Mo Surface Dopants in Enhancing the Orr Performance of Octahedral PtNi Nanoparticles. *Nano Lett.* **2018**, *18*, 798−804.
(25) Snyder, J.; Fujita, T.; Chen, M. W.; Erlebacher, J. Oxygen Reduction in Nanoporous Metal-Ionic Liquid Composite Electrocatalysts. *Nat. Mater.* **2010**, *9*, 904−907.
(26) Snyder, J.; Livi, K.; Erlebacher, J. Oxygen Reduction Reaction Performance of [Mtbd][Beti] Encapsulated Nanoporous Nipt Alloy Nanoparticles. *Adv. Funct. Mater.* **2013**, *23*, 5494−5501.
(27) Zhang, G.-R.; Munoz, M.; Etzold, B. J. Boosting Performance of Low Temperature Fuel Cell Catalysts by Subtle Ionic Liquid Modification. *ACS Appl. Mater. Interfaces* **2015**, *7*, 3562−3570.
(28) Pham Truong, T. N.; Randriamahazaka, H.; Ghilane, J. Polymer Brushes Ionic Liquid as a Catalyst for Oxygen Reduction and Oxygen Evolution Reactions. *ACS Catal.* **2018**, *8*, 869−875.
(29) Kernchen, U.; Etzold, B.; Korth, W.; Jess, A. Solid Catalyst with Ionic Liquid Layer (SCILL) − a New Concept to Improve Selectivity Illustrated by Hydrogenation of Cyclooctadiene. *Chem. Eng. Technol.* **2007**, *30*, 985−994.
(30) Zhang, G. R.; Munoz, M.; Etzold, B. J. Accelerating Oxygen Reduction Catalysts through Preventing Poisoning with Non Reactive Species by Using Hydrophobic Ionic Liquids. *Angew. Chem., Int. Ed.* **2016**, *55*, 2257−2261.
(31) Zhang, G.-R.; Wolker, T.; Sandbeck, D. J.; Munoz, M.; Mayrhofer, K. J.; Cherevko, S.; Etzold, B. J. Tuning the Electrocatalytic Performance of Ionic Liquid Modified Pt Catalysts for Oxygen Reduction Reaction Via Cationic Chain Engineering. *ACS Catal.* **2018**, *8*, 8244−8254.
(32) Huang, X.; Zhao, Z.; Cao, L.; Chen, Y.; Zhu, E.; Lin, Z.; Li, M.; Yan, A.; Zettl, A.; Wang, Y. M.; Duan, X.; Mueller, T.; Huang, Y. High-Performance Transition Metal−Doped Pt3Ni Octahedra for Oxygen Reduction Reaction. *Science* **2015**, *348*, 1230−1234.
(33) Cui, C. H.; Gan, L.; Heggen, M.; Rudi, S.; Strasser, P. Compositional Segregation in Shaped Pt Alloy Nanoparticles and Their Structural Behaviour During Electrocatalysis. *Nat. Mater.* **2013**, *12*, 765−771.
(34) Carpenter, M. K.; Moylan, T. E.; Kukreja, R. S.; Atwan, M. H.; Tessema, M. M. Solvothermal Synthesis of Platinum Alloy Nanoparticles for Oxygen Reduction Electrocatalysis. *J. Am. Chem. Soc.* **2012**, *134*, 8535−8542.
(35) Cherevko, S.; Kulyk, N.; Mayrhofer, K. J. Durability of Platinum-Based Fuel Cell Electrocatalysts: Dissolution of Bulk and Nanoscale Platinum. *Nano Energy* **2016**, *29*, 275−298.
(36) Keeley, G. P.; Cherevko, S.; Mayrhofer, K. J. The Stability Challenge on the Pathway to Low and Ultra Low Platinum Loading for Oxygen Reduction in Fuel Cells. *ChemElectroChem* **2016**, *3*, 51−54.
(37) Martinaiou, I.; Wolker, T.; Shahraei, A.; Zhang, G.-R.; Janßen, A.; Wagner, S.; Weidler, N.; Stark, R. W.; Etzold, B. J.; Kramm, U. I. Improved Electrochemical Performance of Fe-N-C Catalysts through Ionic Liquid Modification in Alkaline Media. *J. Power Sources* **2018**, *375*, 222−232.
(38) Meier, J. C.; Galeano, C.; Katsounaros, I.; Witte, J.; Bongard, H. J.; Topalov, A. A.; Baldizzone, C.; Mezzavilla, S.; Schuth, F.; Mayrhofer, K. J. J. Design Criteria for Stable Pt/C Fuel Cell Catalysts. *Beilstein J. Nanotechnol.* **2014**, *5*, 44−67.
(39) Mayrhofer, K. J. J.; Blizanac, B. B.; Arenz, M.; Stamenkovic, V. R.; Ross, P. N.; Markovic, N. M. The Impact of Geometric and Surface Electronic Properties of Pt-Catalysts on the Particle Size Effect in Electrocatalysis. *J. Phys. Chem. B* **2005**, *109*, 14433−14440.
(40) Buzzeo, M. C.; Evans, R. G.; Compton, R. G. Non Haloaluminate Room Temperature Ionic Liquids in Electrochemistry—a Review. *ChemPhysChem* **2004**, *5*, 1106−1120.
(41) Evans, R. G.; Klymenko, O. V.; Hardacre, C.; Seddon, K. R.; Compton, R. G. Oxidation of N, N, N′, N′-Tetraalkyl-Para-Phenylenediamines in a Series of Room Temperature Ionic Liquids Incorporating the Bis (Trifluoromethylsulfonyl) Imide Anion. *J. Electroanal. Chem.* **2003**, *556*, 179−188.
(42) Suarez, P. A.; Consorti, C. S.; Souza, R. F. d.; Dupont, J.; Gonçalves, R. S. Electrochemical Behavior of Vitreous Glass Carbon and Platinum Electrodes in the Ionic Liquid 1-N-Butyl-3-Methylimidazolium Trifluoroacetate. *J. Braz. Chem. Soc.* **2002**, *13*, 106−109.
(43) Solla-Gullon, J.; Rodriguez, P.; Herrero, E.; Aldaz, A.; Feliu, J. M. Surface Characterization of Platinum Electrodes. *Phys. Chem. Chem. Phys.* **2008**, *10*, 1359−1373.
(44) Vidal-Iglesias, F. J.; Arán-Ais, R. M.; Solla-Gullón, J.; Herrero, E.; Feliu, J. M. Electrochemical Characterization of Shape-Controlled Pt Nanoparticles in Different Supporting Electrolytes. *ACS Catal.* **2012**, *2*, 901−910.
(45) Chen, Q.-S.; Vidal-Iglesias, F. J.; Solla-Gullón, J.; Sun, S.-G.; Feliu, J. M. Role of Surface Defect Sites: From Pt Model Surfaces to Shape-Controlled Nanoparticles. *Chem. Sci.* **2012**, *3*, 136−147.
(46) Cherevko, S.; Keeley, G. P.; Geiger, S.; Zeradjanin, A. R.; Hodnik, N.; Kulyk, N.; Mayrhofer, K. J. J. Dissolution of Platinum in the Operational Range of Fuel Cells. *ChemElectroChem* **2015**, *2*, 1471−1478.
(47) Sanlı, A. e. E.; Aytaç, A. Electrochemistry of the Nickel Electrode as a Cathode Catalyst in the Media of Acidic Peroxide for Application of the Peroxide Fuel Cell. *ECS Trans.* **2011**, *42*, 3−22.

DOI: 10.1021/acscatal.9b01772
ACS Catal. 2019, 9, 8682−8692

(48) De Vito, E.; Marcus, P. Xps Study of Passive Films Formed on Molybdenum-Implanted Austenitic Stainless Steels. *Surf. Interface Anal.* **1992**, *19*, 403−408.
(49) Popa, M. V.; Vasilescu, E.; Drob, P.; Vasilescu, C.; Mirza-Rosca, J.; Lopez, A. S. Corrosion Behavior of Some Titanium Base Alloys in Acid Solutions. *Mater. Manuf. Processes* **2005**, *20*, 35−45.
(50) Maurice, V.; Peng, H.; Klein, L. H.; Seyeux, A.; Zanna, S.; Marcus, P. Effects of Molybdenum on the Composition and Nanoscale Morphology of Passivated Austenitic Stainless Steel Surfaces. *Faraday Discuss.* **2015**, *180*, 151−170.
(51) Abbott, A. P.; Frisch, G.; Hartley, J.; Karim, W. O.; Ryder, K. S. Anodic Dissolution of Metals in Ionic Liquids. *Prog. Nat. Sci.* **2015**, *25*, 595−602.
(52) Quijada-Maldonado, E.; Sánchez, F.; Pérez, B.; Tapia, R.; Romero, J. Task-Specific Ionic Liquids as Extractants for the Solvent Extraction of Molybdenum(Vi) from Aqueous Solution Using Different Commercial Ionic Liquids as Diluents. *Ind. Eng. Chem. Res.* **2018**, *57*, 1621−1629.
(53) Visser, A. E.; Swatloski, R. P.; Reichert, W. M.; Mayton, R.; Sheff, S.; Wierzbicki, A.; Davis, J. J. H.; Rogers, R. D. Task-Specific Ionic Liquids for the Extraction of Metal Ions from Aqueous Solutions. *Chem. Commun.* **2001**, 135−136.
(54) de los Ríos, A. P.; Hernández-Fernández, F. J.; Lozano, L. J.; Sánchez, S.; Moreno, J. I.; Godínez, C. Removal of Metal Ions from Aqueous Solutions by Extraction with Ionic Liquids. *J. Chem. Eng. Data* **2010**, *55*, 605−608.
(55) Dupont, D.; Raiguel, S.; Binnemans, K. Sulfonic Acid Functionalized Ionic Liquids for Dissolution of Metal Oxides and Solvent Extraction of Metal Ions. *Chem. Commun.* **2015**, *51*, 9006−9009.
(56) Nockemann, P.; Thijs, B.; Pittois, S.; Thoen, J.; Glorieux, C.; Van Hecke, K.; Van Meervelt, L.; Kirchner, B.; Binnemans, K. Task-Specific Ionic Liquid for Solubilizing Metal Oxides. *J. Phys. Chem. B* **2006**, *110*, 20978−20992.
(57) Saji, V. S.; Lee, C.-W. Molybdenum, Molybdenum Oxides, and Their Electrochemistry. *ChemSusChem* **2012**, *5*, 1146−1161.
(58) Pareek, A.; Ankah, G. N.; Cherevko, S.; Ebbinghaus, P.; Mayrhofer, K. J. J.; Erbe, A.; Renner, F. U. Effect of Thiol Self-Assembled Monolayers and Plasma Polymer Films on Dealloying of Cu−Au Alloys. *RSC Adv.* **2013**, *3*, 6586−6595.
(59) Ankah, G. N.; Pareek, A.; Cherevko, S.; Zegenhagen, J.; Renner, F. U. Hierarchical Nanoporous Films Obtained by Surface Cracking on Cu-Au and Ethanethiol on Au(001). *Electrochim. Acta* **2014**, *140*, 352−358.
(60) Mayrhofer, K. J. J.; Juhart, V.; Hartl, K.; Hanzlik, M.; Arenz, M. Adsorbate-Induced Surface Segregation for Core−Shell Nanocatalysts. *Angew. Chem., Int. Ed.* **2009**, *48*, 3529−3531.

DOI: 10.1021/acscatal.9b01772
ACS Catal. 2019, 9, 8682−8692